Available online at www.sciencedirect.com
ScienceDirect
Journal of Power Sources 159 (2006) 943–950
JOURNAL OF POWER SOURCES
www.elsevier.com/locate/jpowsour

Analysis and modeling of PEM fuel cell stack performance: Effect of in situ reverse water gas shift reaction and oxygen bleeding

G. Karimi[1], Xianguo Li*

Department of Mechanical Engineering, University of Waterloo, Waterloo, Ont., Canada N2L 3G1

Received 26 September 2005; accepted 19 November 2005
Available online 22 May 2006

Abstract

In this study the performance of a polymer electrolyte membrane (PEM) fuel cell stack is analyzed with a mathematical model when the stack operates on hydrocarbon reformate gas as the anode feed stream. It is shown that the effect of carbon dioxide dilution of the hydrogen dominated reformate gas has a minimal impact on the stack performance. However, the CO-poisoning effect due to the in situ reverse water gas shift reaction in the anode feed stream could have a very serious adverse impact on the stack performance, especially at high current densities. Thermodynamic calculations indicate that the equilibrium concentrations of CO could be as high as 100 ppm, generated by the in situ reverse water gas shift reaction, under the typical conditions of PEM fuel cell operation; and are influenced by the stack operating temperature and water content of the reformate anode feed. This CO-poisoning of the stack performance is shown mitigated effectively by introducing about 0.5–1% oxygen to the anode feed.

Keywords: PEM fuel cell; Stack; Reformate fuel; CO-poisoning; Reverse water gas shift reaction; Mathematical modeling

1. Introduction

Environmental concerns and diminishing fossil fuel reserves are generating demand for new energy conversion technologies that can provide improved or alternative methods of energy conversion and power generation. Polymer electrolyte membrane (PEM) fuel cells are widely regarded as alternative stationary and mobile power sources with potentially zero or minimal environmental impact. In PEM fuel cells, the chemical energy of hydrogen and oxygen is converted directly and efficiently into electrical energy, with only waste heat and liquid water as by-products. Although the preferred fuel for the operation of low temperature PEM fuel cells is pure hydrogen, on-board/on-site hydrogen generation seems to be a viable transitional solution for the near-term introduction of fuel cells due to a lack of infrastructure and technical challenges to be overcome for hydrogen production, storage and delivery.

In a fuel cell system, hydrogen is generated by the consecutive reforming and cleaning of carbon-based fuels such as gasoline, natural gas or methanol. This will lead to fuel cell fuels containing hydrogen with concentration of only 30–75%, depending on the primary fuel used and the reforming process employed [1–3]. The other gas components are carbon dioxide, nitrogen, water, incompletely converted fuel and carbon monoxide [4,5], while trace amounts of ammonia, hydrogen cyanide and hydrogen sulfide are reported as well [6]. The detrimental effect of small amounts of CO (at ppm levels) on the cell performance, referred to as CO-poisoning, is well known as this chemical hinders hydrogen oxidation in the anode and results in a severe decrease in fuel cell energy conversion efficiency. Oxygen bleeding is one of the most effective means of mitigation of CO-poisoning in which the anode fuel is injected with 1–4% oxygen [7]. While CO_2 itself is regarded as inert, the formation of carbon monoxide by a reverse water gas shift reaction leads to a negative impact of carbon dioxide on the performance of fuel cell anodes. As the concentration of carbon dioxide is of the order of up to 25%, a very small reverse water gas shift can lead to carbon monoxide concentrations which are comparable to the concentration directly emitted by the fuel cell processor, up to a concentration level of 10–100 ppm [8,9].

* Corresponding author: Tel.: +1 519 888 4567; fax: +1 519 885 5862.
[1] Present address: Department of Chemical Engineering, Shiraz University, Shiraz, Iran.
E-mail address: x6li@uwaterloo.ca (X. Li).

0378-7753/$ – see front matter © 2006 Elsevier B.V. All rights reserved.
doi:10.1016/j.jpowsour.2005.11.104

Nomenclature

A	cell area (m^2)
C	molar concentration ($mol\,l^{-1}$)
D	diffusion coefficient ($m^2\,s^{-1}$)
D_h	manifold hydraulic diameter (m)
E	cell or stack voltage (V)
f_{PT}	mass ratio of platinum to carbon support
F	Faraday constant ($96485\,C\,mole^{-1}$)
H	bipolar plate effective height (m)
J	cell current density ($A\,cm^{-2}$)
K_E	electrokinetic permeability of proton exchange membrane (m^2)
K_p	hydraulic permeability of proton exchange membrane (m^2)
l	flow channel length (m)
l_m	fraction of catalyst layer void space occupied by liquid water
m_{pt}	platinum mass loading per unit electrode area ($kg\,m^{-2}$)
N	number of cells/flow channels/turns
$\dot{N}$	molar flow rate ($mol\,s^{-1}$)
$\dot{N}_r$	rate of reactant consumption/production in the catalyst layer ($mol\,s^{-1}$)
P	pressure (atm)
S	stoichiometry
T	stack temperature (K)
W	bipolar plate effective width (m)
y	mole fraction

Greek letters

η	overpotential (V)
κ_s	conductivity of catalyst layer solid phase ($S\,m^{-1}$)
ρ_e^{bulk}	resistivity of electrode backing ($\Omega\,m$)
ϕ	porosity

Subscripts

a	anode
bp	bipolar plate
c	cathode/flow channel/catalyst layer
cell	fuel cell
CO	carbon monoxide
CO_2	carbon dioxide
cp	cooling plate
e	electrode backing
eq	equilibrium condition
H_2	hydrogen
i	component
in	inlet
m	membrane
out	out/outlet value
O_2	oxygen
r	reacting
rev	reversible
stack	stack

The aim of this paper is to investigate further the damaging effect of the CO poisoning induced by the reverse water gas shift reaction in the anode fuel stream, as well as the interplay with O_2-bleeding. In particular, model studies are carried out for a PEM fuel cell stack operating under conditions relevant to stationary and mobile applications. The concentration of CO is determined as a function of cell temperature and the anode fuel composition. To this end, we have combined a recently developed single cell model [10] which describes the kinetics of H_2 electro-oxidation in the presence of CO and O_2 with a recently developed stack flow network model [11], to analyze the stack performance over a wide range of operating conditions with hydrocarbon reformate gas as fuel.

2. Model formulations

A cross-section of a typical fuel cell stack is shown in Fig. 1. The individual cells, referred to as membrane electrode assemblies (MEA), are composed of a membrane electrolyte sandwiched between two porous electrodes. The MEAs produce direct current electricity. Bipolar plates which are electrically conducting, separate the MEAs as well as providing a means for delivery of the fuel and oxidant to the catalyst layer at the electrode–membrane interface. The basic unit is repeated to build up a stack. A complete multi-cell stack may include cooling plates to remove heat from the stack and provide a uniform stack temperature.

The fuel and oxidant for each PEM fuel cell are supplied by the main inlets through the stack manifold, with the anode manifold supplying fuel and the cathode manifold supplying oxidant. For a PEM fuel cell stack operating with reformate fuel, the main anode components are H_2 and CO_2. Traces of CO may also be present due to an incomplete cleaning process. The oxidant used in a PEM fuel cell is O_2 accompanied with N_2 if air is used for the oxygen supply. The inlet streams are usually humidified. The gas flow channels distribute the reactants to the fuel cells, remove the water produced by the electrochemical reactions within the membrane electrode assembly and supply the humidity required to avoid proton exchange membrane from

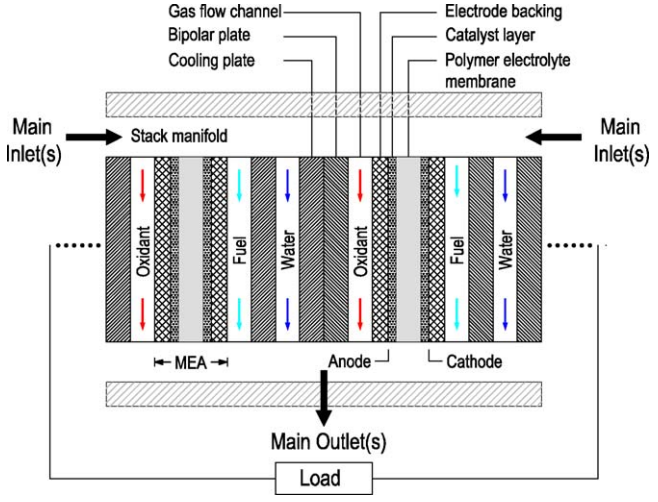

Fig. 1. Schematic of a portion of a PEM fuel cell stack.

dehydration. In addition to fuel and oxidant, water is circulated through cooling plates in order to remove the heat produced by the PEM fuel cells and hence in this study a constant temperature within the stack is considered. In practice, a uniform temperature throughout the stack is hardly ever achieved, and typical variations of a few degrees from cell to cell and within a cell are likely. As a result, stack performance suffers. The effect of non-uniform temperature distribution and the related cooling issue will be investigated in a future study, building upon the present work. It is known that thermal management is one of the two critical issues for PEM fuel cells.

The stack performance, often measured in terms of the stack voltage, E_{stack}, can be determined by

$$E_{\text{stack}} = \sum_{1}^{N_{\text{cell}}} E_{\text{cell}} - \sum_{1}^{N_{\text{cell}}} \eta_{\text{cp}} \tag{1}$$

where N_{cell} is the total number of fuel cells in the stack, E_{cell} the voltage of each cell, and η_{cp} is the ohmic loss due to a cooling plate.

The stack model presented here consists of two parts: the stack flow network model and the single cell model. The distribution of the reactants and products molar flow rates, pressure, and compositions in the flow channels are determined using the stack flow model as a function of the anode and cathode stoichiometries, current density and stack design parameters. The single cell model determines the voltage of each cell in the stack based on these distributions.

2.1. Stack flow network model

A novel flow network model was developed recently by the authors to optimize the performance of a H_2/air PEM fuel cell stack with various inlet–outlet configurations and over a wide range of design and operating conditions [11]. In the stack model, several independent loops are considered for the fuel and oxidant streams, with each loop comprising a number of control volumes to characterize the manifolds and gas flow channels. The pressure and compositions are considered to be uniform in each control volume. Mass transfers due to electrochemical reactions are calculated at average operating conditions (logarithmic mean) which prevails in the flow channels. In this study, the same flow network model is further improved for the anode side of the stack to handle reformate fuel and to account for the reverse water gas shift reaction and possible O_2-bleeding for mitigation of CO-poisoning. Since it is described in detail elsewhere, this section only highlights the major assumptions, methodologies and new features of the stack flow network model.

The inlet hydrogen and oxygen molar flow rates required for the stack operation are determined by

$$\dot{N}_{\text{H}_2}^{\text{stack}} = \frac{S_{\text{a}} N_{\text{cell}} J A_{\text{cell}}}{2F}, \qquad \dot{N}_{\text{O}_2}^{\text{stack}} = \frac{S_{\text{c}} N_{\text{cell}} J A_{\text{cell}}}{4F}$$

where S_{a} and S_{c} are the stack anode and cathode stoichiometries, respectively, J is the cell current density, A_{cell} is the active cell area and F is the Faraday's constant. Total inlet molar flow rates are calculated by adding the carbon dioxide, water vapor and nitrogen to the inlet streams. Oxygen will also be accounted for if oxygen bleeding is performed for mitigation of CO-poisoning in the anode side of the stack. The maximum amount of water vapor coming into the stack with the reactants corresponds to 100% relative humidity in the incoming gas streams.

The distribution of incoming components into the individual cells is governed by conservation laws. Conservation of mass requires that the molar flow rates into and out of each control volume be balanced with the reactant consumptions and reaction products. As illustrated in Fig. 2, fuel and oxidant streams enter the gas flow channels at location 1 with a molar flow rate of $\dot{N}_{i,\text{in}}$ and concentration of $C_{i,\text{in}}$. In the anode side, reactants enter the electrode backing at a molar flow rate $\dot{N}_{\text{r}}$, calculated by Faraday's law [12].

$$\frac{J A_{\text{cell}}}{2F} = \dot{N}_{\text{H}_2,\text{r}} + \dot{N}_{\text{CO,r}} - 2\dot{N}_{\text{O}_2,\text{r}} \tag{2}$$

where $\dot{N}_{\text{CO,r}}$ and $\dot{N}_{\text{O}_2,\text{r}}$ are the molar flow rates of CO and O_2 accessible to the anodic catalyst layer. Carbon monoxide may be present in the inlet fuel stream and can be produced through the reverse water gas shift reaction. For a PEM fuel cell stack operating with CO-free reformate fuel, the main components are H_2 and CO_2, normally fully humidified. The coexistence of H_2, CO_2 and water vapor in the gas flow channels can induce water gas shift reaction and results in trace concentrations of CO in the anode. The water gas shift reaction is a weakly exothermic, reversible reaction in accordance with the following reaction equation:

$$\text{H}_2\text{O(g)} + \text{CO(g)} \rightleftharpoons \text{H}_2\text{(g)} + \text{CO}_2\text{(g)} \tag{3}$$

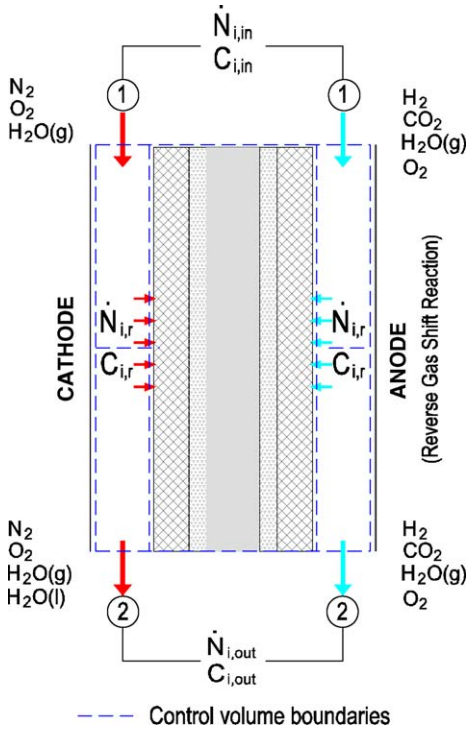

Fig. 2. Schematic of flow channels surrounding a single PEM fuel cell in the stack.

The equilibrium concentration of CO resulting from the reaction of CO_2 and H_2 can be calculated from the equilibrium constant of the water gas shift reaction [13]:

$$\ln(K_{eq}) = \frac{5693.5}{T} + 1.077 \ln T + 5.44 \times 10^{-4} T - 1.125 \times 10^{-7} T^2 - \frac{49170}{T^2} - 13.148 \quad (4)$$

where T is the operating temperature (in K). The equilibrium constant, K_{eq}, can be related to the mole fractions of components, y:

$$K_{eq} = \frac{y_{H_2} y_{CO_2}}{y_{H_2O} y_{CO}} \quad (5)$$

Although the equilibrium constant represented by Eq. (4) is a sensitive function of temperature, the CO concentration from the reverse water gas shift reaction varies with the molar composition of the components present in the reformate fuel. The equilibrium constant decreases with temperature from 8800 at 80 °C to 4136 at 100 °C. For a fuel containing 75% H_2 and 25% CO_2 (dry basis), representative for a methanol-based reformate, the equilibrium conversion of the water gas shift reaction can be calculated. Fig. 3 shows the exiting CO concentration under equilibrium conversion as a function of stack operating pressure and level of humidification at a temperature of 80 °C. According to this figure, lower pressure and higher fuel humidification will result in a lower CO concentration. This is reasonable because at lower pressure, reformate fuel can hold a larger amount of water vapor and a larger level of humidification (relative humidity) means a larger water mole fraction (y_{H_2O}), both of which tend to shift the equilibrium towards the CO elimination (to the right direction in Eq. (3)). The most important conclusion which can be drawn from Fig. 3 is that, based on thermodynamics, the CO being produced by the reverse water gas shift reaction taking place in the fuel cell itself, could be in the range of up to 100 ppm, higher than the CO outlet from the fuel processor system with selective oxidation unit which can lower the CO concentration to/within 10 ppm range. This is in complete agreement with the estimated CO concentrations reported recently by de Bruijn et al. [9].

The H_2 fuel along with the CO produced by the homogeneous reverse water gas shift reaction and O_2 (if supplied for bleeding) diffuse through the electrode backing and brought into contact with the anode catalyst layer where adsorption, desorption and electro-oxidation of H_2 and CO, as well as the heterogeneous oxidation of CO and H_2 by O_2 take place [10], and the produced protons migrate through the electrolyte membrane towards the cathode side.

In the cathode side, the species present are O_2, N_2 and H_2O. Nitrogen does not react in the cathode catalyst layer. The amount of O_2 consumed and H_2O produced can be determined by Faraday's law:

$$\dot{N}_{O_2,r} = \frac{JA_{cell}}{4F} \quad \text{and} \quad \dot{N}_{H_2O,r} = 2\dot{N}_{O_2,r} \quad (6)$$

Further, the net water transport through the membrane electrolyte is taken into account [11]. As with the anode catalyst layer, conservation of species, diffusion and Ohm's laws, and reaction kinetics are applied to generate the governing equations of the cathode catalyst layer. The details of fuel cell mass transfer and reaction kinetics can be found in [10,14].

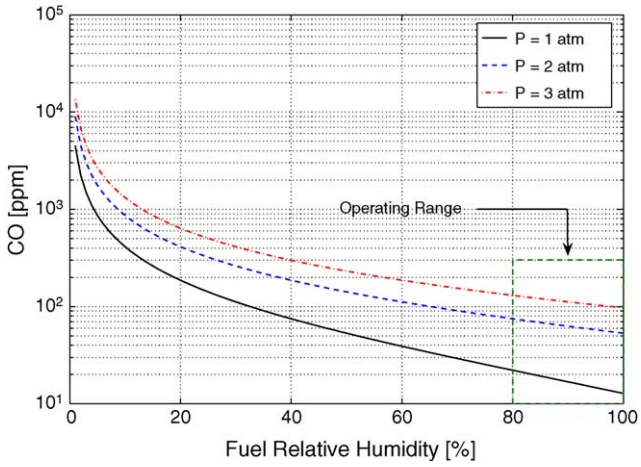

Fig. 3. Equilibrium CO mole fraction (in terms of ppm) as functions of fuel humidification level and operating pressure (based on a reformate fuel comprising of 75% H_2 and 25% CO_2—dry basis, at 80 °C).

The conservation of energy equation dictates that the sum of the pressure losses in each loop of the stack be zero. The pressure losses are related to the molar flow rates. The set of non-linear relationship between the pressure losses and mass flow rates in the stack manifolds and gas flow channels are solved using an iterative technique. The solution of the stack flow network model provides the molar flow rate distributions, composition and pressure in the flow channels. These values are used by the single cell model to calculate the voltage of each cell in the stack as follows.

2.2. Single cell model

The voltage of each cell in the stack is calculated using the single cell model developed by Baschuk and Li [10]. According to this model, the output voltage of a single cell can be determined as follows:

$$E_{cell} = E_{rev} - \eta_a - |\eta_c| - 2\eta_{bp} - 2\eta_e - \eta_m \quad (7)$$

where E_{rev} is the reversible cell voltage, η_a and η_c are the overpotentials attributed to the anode and cathode catalyst layers. The voltage losses caused by the bipolar plate, electrode backing and proton exchange membrane are denoted by η_{bp}, η_e, and η_m, respectively.

The reversible cell voltage is the cell potential obtained at thermodynamic equilibrium. It is a function of temperature and reactant concentration through a modified version of the Nernst equation. The actual cell voltage is determined from the reversible cell voltage minus the overpotentials occurred in the various components of the PEM fuel cell. The anode and cathode catalyst layer overpotentials are found by considering species conservation, and proton and electron migration within the catalyst layers. Proton and electron migration through the catalyst layers are related to the protonic and electrical current using

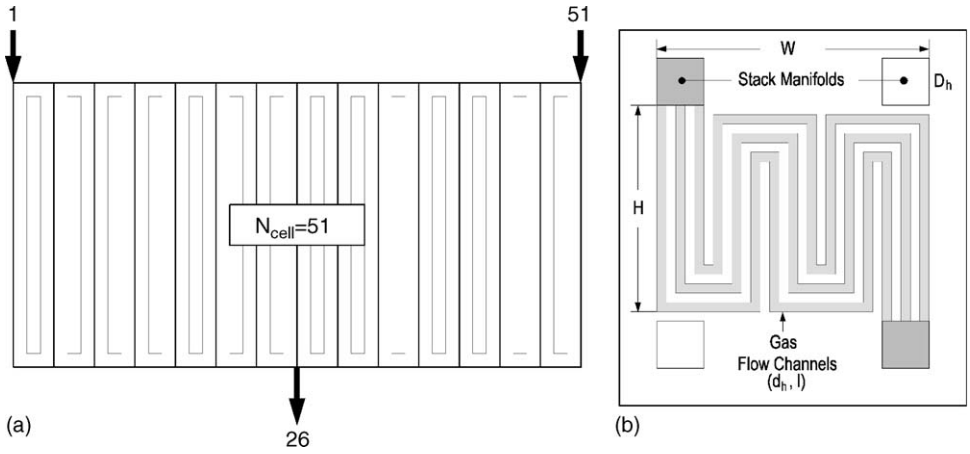

Fig. 4. Schematics of (a) a typical PEM fuel cell stack with symmetric two-inlets one-outlet configuration and (b) a bipolar plate with serpentine flow channel configuration and three flow channels per plate.

Ohm's law. Species conservation requires modeling of reaction kinetics and mass transport. Oxygen reduction is modeled with the Butler–Volmer equation in the cathode catalyst layer, while in the anode catalyst layer the adsorption and desorption of H_2, CO, and O_2, the electro-oxidation of the adsorbed hydrogen and carbon monoxide, and the heterogeneous oxidation of H_2 and CO by O_2 are included in the reaction kinetics. The voltage losses attributed to the bipolar plate and electrode backing are the result of electron migration and calculated using Ohm's law. The overpotential associated with the proton migration in the proton exchange membrane is determined by the Nernst–Planck equation assuming a constant conductivity for the fully hydrated proton exchange membrane.

Determination of the reversible cell voltage and overpotentials requires several operating and design parameters such as conductivity, porosity and geometric dimensions. The operating parameters include current density, temperature, pressure, reactant composition and stoichiometry.

Due to the series connection, the current density in each cell will be equal. As explained early, the circulation of cooling water is considered to maintain a uniform temperature for each cell in the stack, leaving the effect of non-uniform temperature to a future study. However, the pressure, reactant composition and stoichiometry can vary from cell to cell if the mass flow rate and pressure distributions within the stack are unequal; this variation is analyzed with the stack flow model described earlier.

3. Results and discussion

The input parameters for the fuel cell stack are classified as operating and design parameters. The design parameters are the fuel cell size, stack manifold and flow channel dimensions and configuration. Operating parameters include the stack current density, temperature, pressure, stoichiometry and the reactant composition at the stack inlet(s). Table 1 lists a summary of the operating and relevant design parameters for various cell and stack components such as the bipolar plate, electrode backing, catalyst layer and polymer electrolyte membrane. The schematic of a typical PEM fuel cell stack containing 51 cells and the bipolar plates used in the present study are illustrated in Fig. 4. Symmetric two-inlet one-outlet configurations are used for both anode and cathode sides since it will maximize the fuel cell stack performance [11]. The numerical technique used in the present model study has been described in [11].

The logarithmic average of reactant concentrations along with the pressure distributions in the stack flow channels are calculated and used in the single cell model to calculate stack voltage distributions. Stack temperature is considered to be constant at 80 °C. Fig. 5 shows the variations of cell-to-cell voltage distributions as a function of current density for a fuel cell stack operating with pure H_2 and air. As indicated in this figure, the cell voltage is maximum near the stack inlets due to the larger concentrations of the fuel and oxidant there and decreases as

Table 1
Parameters and properties used in the present PEM fuel cell stack simulations

Component	Parameter	Value
Bipolar plate	W	0.12 m
	H	0.12 m
	l	0.3 m
	d_h	2×10^{-3} m
	D_h	0.01 m
	N_c	10
Electrode backing[a]	ρ_e^{bulk}	6×10^{-5} Ωm
	δ_e	2.5×10^{-4} m
	ϕ_e	0.4
Catalyst layer[a]	δ_c	2.0465×10^{-5} m
	m_{pt}	0.004 kg m^2
	f_{pt}	0.2
	l_m	0.9
	κ_s	72700 S m^{-1}
Polymer electrolyte membrane[a]	δ_m	1.64×10^{-4} m
	K_E	7.18×10^{-20} m^2
	K_p	1.8×10^{-18} m^2
	C_{H^+}	1200 mol m^{-3}
	D_{H^+}	4.5×10^{-9} m^2 s^{-2}
Stack	N_{cells}	51
	N_{inlets}	2
	T	353 K
	P_{out}	1 atm
	J	0–1 A cm^{-2}
	S_a	1.2
	S_c	2.0

[a] Parameters associated with the single cell model [10].

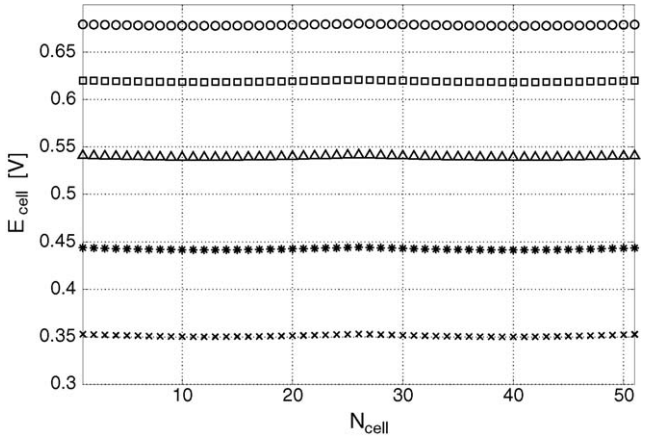

Fig. 5. Variations of cell-to-cell voltage distributions as a function of current density for a fuel cell stack operating with pure H_2/air at the current density of 0.1 (○), 0.2 (□), 0.4 (△), 0.7 (∗) and 1.0 A cm^{-2} (×).

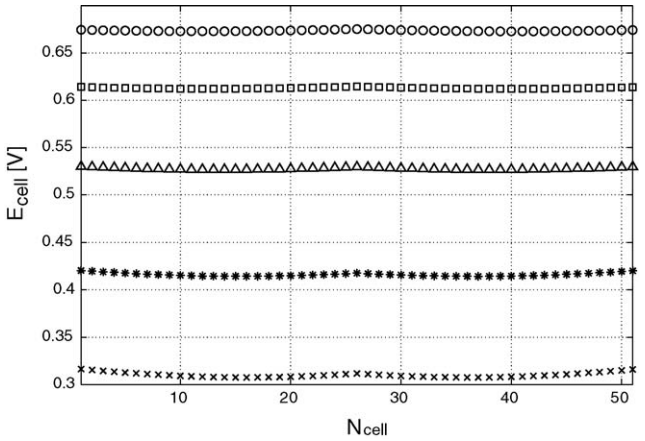

Fig. 6. Variations of cell-to-cell voltage distributions as a function of current density for a fuel cell stack operating with reformate fuel (75% H_2, 25% CO_2—dry basis)/air at the current density of 0.1 (○), 0.2 (□), 0.4 (△), 0.7 (∗) and 1.0 A cm^{-2} (×).

the distance from the inlet increases. However, the cell-to-cell voltage distribution is very small due to the large flow channels-to-manifolds flow resistance in both anode and cathode sides of the fuel cell stack as pointed out recently [11]. The stack voltage is a strong function of the current density J. The stack voltage is reduced by 52% when J is increased from 0.1 to 1 A cm^{-2} due mainly to the ohmic and concentration overpotentials.

The effects of the CO_2 dilution on the stack voltage is shown in Fig. 6. A fully humidified reformate fuel with 75% H_2 and 25% CO_2 (dry basis) and air were utilized in the absence of the water gas shift reaction. It is seen that the presence of the CO_2 in the anode side of the stack will hinder the transport of H_2 to the anodic catalyst layer and degrades the stack performance, an effect often referred to as the dilution effect. The stack voltage is reduced by 0.5% at 0.1 A cm^{-2} to 12% at 1 A cm^{-2}. Clearly, the cell voltage distribution becomes more non-uniform for the reformate fuel as compared to the pure hydrogen case shown in Fig. 5, particularly at higher current densities. This is because for the reformate fuel, the total fuel stream flow rate is increased significantly for the given hydrogen stoichiometry; and this increased total flow causes significantly non-uniform flow of the fuel stream among the cells in the stack, as shown by Baschuk and Li [16].

The effect of CO-poisoning due to the reverse water gas shift reaction on the stack voltage is very critical. Fig. 7 shows the variations of cell-to-cell voltage distributions as a function of current density for a fuel cell stack operating with reformate fuel (75% H_2, 25% CO_2—dry basis) with traces of CO produced by the reverse water gas shift reaction and air. Although the CO-poisoning at low current densities does not influence the stack operation considerably, the stack will stop working at high current densities. Several reasons exists. As the stack current density is increased, the reactant flow rate as well as the stack pressure increases. The higher stack pressure will results in a higher CO concentration as previously pointed out. In addition, with the higher current density, the mass transfer resistances are increased which in turn influences the stack performance.

The CO-poisoning can be efficiently mitigated by introducing O_2 into the fuel gas stream. Only a few percent of O_2-bleeding can convert the CO into the CO_2 in the catalyst layer and free the reaction sites for H_2 reduction [15]. The PEM fuel cell model used in this study simulates the effect of oxygen bleeding in the fuel cell stack by incorporating the heterogeneous oxidation of carbon monoxide and hydrogen by O_2 [10]. Comparison of Fig. 7 with Fig. 8 clearly shows how the stack performance is upgraded when 4% O_2 is introduced with the reformate fuel. The effect is particularly significant at high current densities (e.g. $J > 0.4$ A cm^{-2}). It is noticed during the present analysis that a mere 0.5% of O_2 in the fuel stream is sufficient to recover the stack performance.

Variations of cell-to-cell averaged H_2 and CO_2 concentration distributions for a fuel cell stack operating with reformate fuel (74.6% H_2, 24.9% CO_2, 0.5% O_2-dry basis) with traces of CO produced by the reverse water gas shift reaction and air are shown in Fig. 9(a) and (b), respectively, as a function of current density. The corresponding average distributions in terms of ppm for CO and O_2 are shown in Fig. 10.(a) and (b). From these figures,

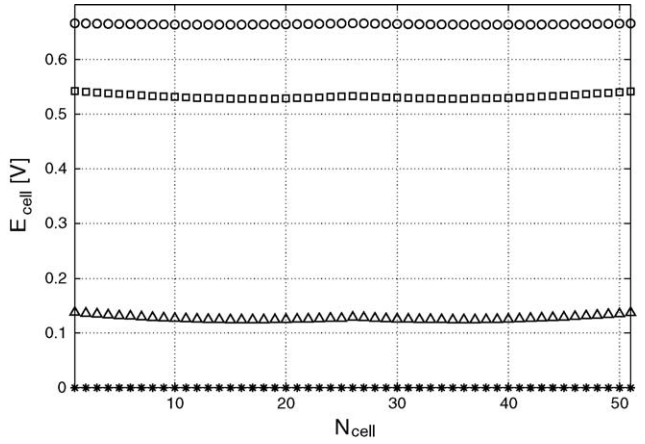

Fig. 7. Variations of cell-to-cell voltage distributions as a function of current density for a fuel cell stack operating with reformate fuel (75% H_2, 25% CO_2—dry basis) with traces of CO produced by the reverse water gas shift reaction/air at the current density of 0.1 (○), 0.2 (□), 0.4 (△), 0.7 (∗) and 1.0 A cm^{-2} (×).

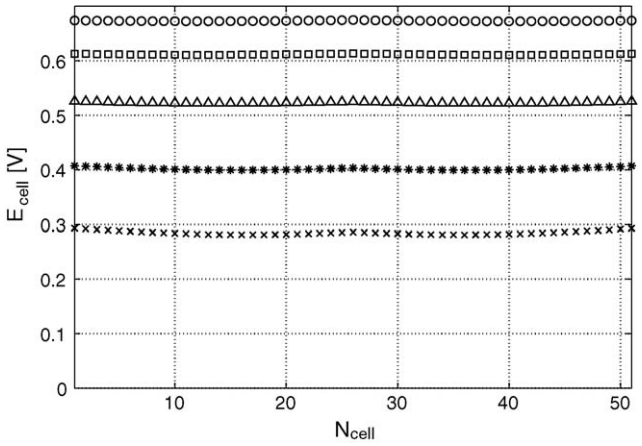

Fig. 8. Variations of cell-to-cell voltage distributions as a function of current density for a fuel cell stack operating with reformate fuel (72% H_2, 24% CO_2, 4% O_2—dry basis) with traces of CO produced by the reverse water gas shift reaction/air at the current density of 0.1 (○), 0.2 (□), 0.4 (△), 0.7 (∗) and 1.0 A cm^{-2} (×).

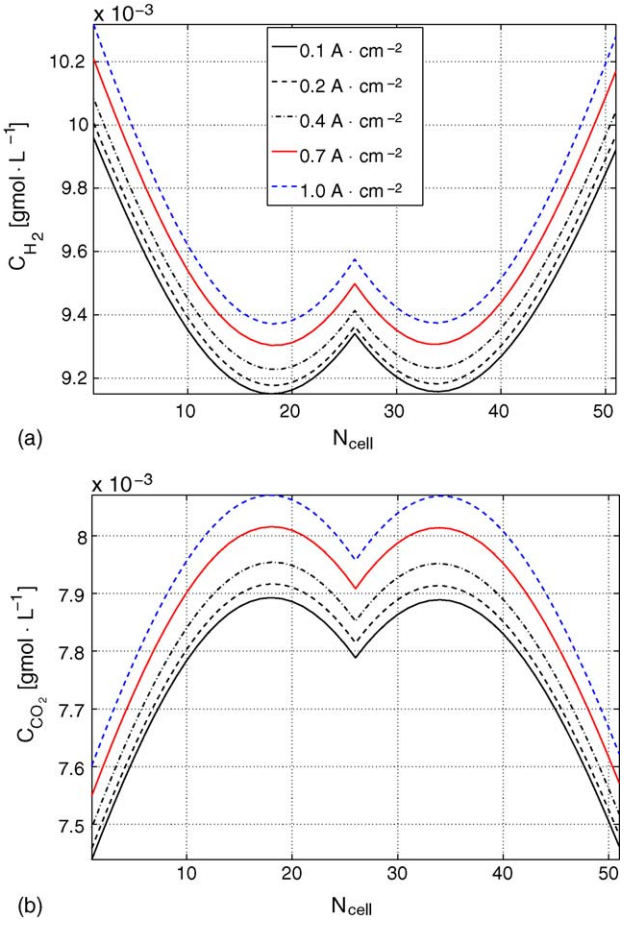

Fig. 9. Variations of cell-to-cell average concentration distributions as a function of current density for a fuel cell stack operating with reformate fuel (74.6% H_2 , 24.9% CO_2 , 0.5% O_2—dry basis) with traces of CO produced by the reverse water gas shift reaction/air. (a) H_2 and (b) CO_2.

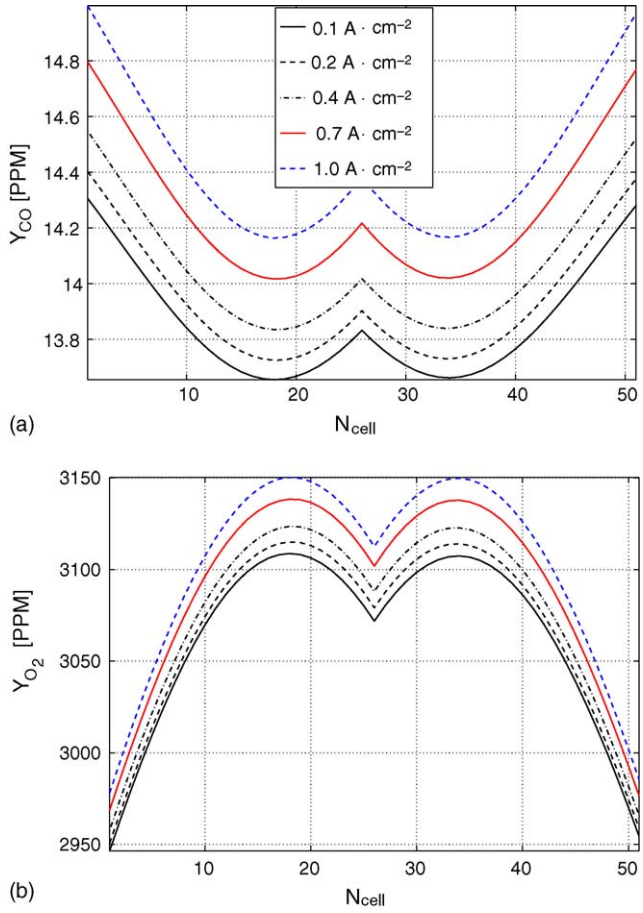

Fig. 10. Variations of cell-to-cell average mole fraction distributions (in terms of ppm) as a function of current density for a fuel cell stack operating with reformate fuel (74.6% H_2, 24.9% CO_2, 0.5% O_2—dry basis) with traces of CO produced by the reverse water gas shift reaction/air. (a) CO and (b) O_2.

the O_2-to-CO concentration ratio varies from about 200 in flow channels near the inlet to about 230 in those located close to the middle of the fuel cell stack. This means that an O_2-to-CO concentration ratio of about 200 is sufficient to mitigate CO-poisoning and recover fully the stack performance. Average O_2 concentration distribution for the cells in the stack is shown in Fig. 11 for the cathode side when air is used as oxidant. The O_2 distribution is very similar to the H_2 in the anode side as shown in Fig. 9(a) earlier.

It should be noted that in Figs. 9–11 the singular peaks that are present at cell number 26 (i.e., the middle cell in the stack considered in this study) are not physical, rather it is a result of the present model with the flow network approach. Another interesting observation is that the present stack configuration shown in Fig. 4 might be considered as two Z configuration stacks being assembled together: one is for the cell numbers from 1 to 26, and the other from 26 to 51. Clearly, the concentration distribution shown in Figs. 9–11 resembles the distribution for Z configuration stacks described in earlier studies [11,16].

Fig. 12 displays the polarization curves for a fuel cell stack operating with different fuel compositions over a wide range of current densities. The initial drop in the stack voltage at low current densities is due to activation overpotential. The stack

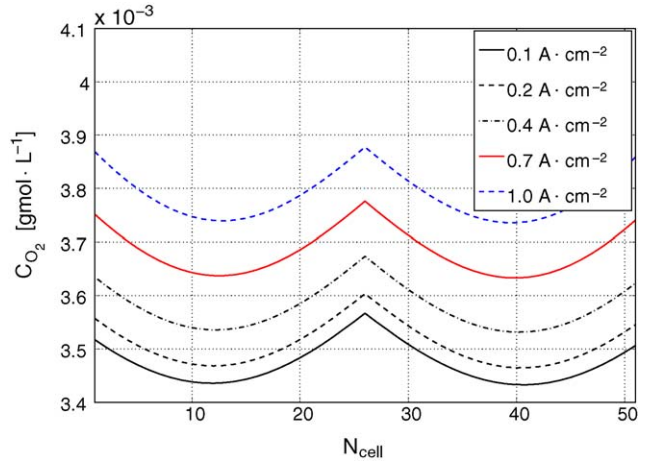

Fig. 11. Variations of cell-to-cell O_2 average concentration distribution as a function of current density in the cathode side of the stack operating with air.

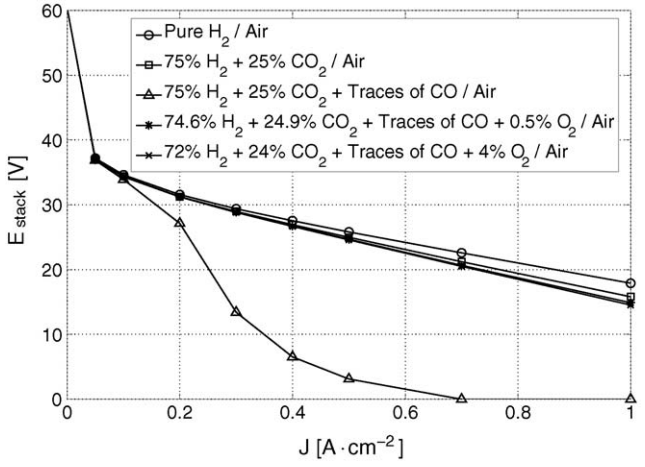

Fig. 12. Polarization curves for a fuel cell stack operating with different fuel compositions.

voltage is reduced linearly for higher current density due to ohmic resistances. Although a PEM fuel cell stack operating with pure hydrogen (fully humidified) and air provides the best performance, modeling results show that the dilution effect due to the presence of the CO_2 in the reformate fuel (up to 75%) does not degrade the stack voltage appreciably. The maximum reduction in the stack voltage is about 12% at 1 A cm^{-2}. This is in agreement with the result of Chinchen et al. [13]. The presence of CO in the reformate fuel due to the reverse water gas shift would bring the stack operation to a halt at current densities above 0.7–1 A cm^{-2}. However, a 0.5% O_2-bleeding will result in a full stack performance recovery. The present modeling results indicate negligible difference between 0.5 and 4% O_2-bleeding.

4. Concluding remarks

The presence of CO_2 in the anode feed of PEM fuel cell stack can lead to a significant loss in performance. The negative effect is caused by the formation of CO via the in situ reverse water gas shift reaction in the bipolar flow channels and the anode electrode structures. Thermodynamic calculations show that the reverse water gas shift reaction can lead to equilibrium concentrations of CO in the range of 20–100 ppm, both temperature and water content of the anode feed are important parameters. This study presented a mathematical model of a PEM fuel cell stack that simulates CO-poisoning and O_2-bleeding. The adsorption, desorption and electro-oxidation of CO and H_2 are modeled by the reactant-pair and Tafel–Volmer mechanism, respectively. Oxygen bleeding is modeled by the heterogeneous oxidation of CO and H_2. It is concluded that CO_2 dilution effect has a minimal impact on the stack performance, a complete removal of CO from reformate fuel cannot guarantee PEM fuel cell stack performance unless about 0.5–1% of O_2 is introduced into the feed. The modeling results show that further addition of oxygen to the reformed fuel does not improve the stack performance and could result in unwanted oxidation of H_2.

Acknowledgements

This work was supported by AUTO21, the Network of Centers of Excellence, Canada. The significant help from J.J. Baschuk for the modification of the single cell code and Dr. J. Park for executing the codes is highly appreciated.

References

[1] J.R. Rostrup-Nielsen, Phys. Chem. 3 (2001) 283.
[2] A. Heinzel, B. Vogel, T. Rampe, A. Haist, P. Hubner, Proceedings of the Seminar on Fuel Cell, Portland, OR, 2000, p. 256.
[3] A. Docter, G. Konrad, A. Lamm, Proceedings of the Seminar on Fuel Cell, Portland, OR, 2000, p. 538.
[4] L.F. Brown, Los Alamos Report No. LA-13112-MS, Los Alamos, 1996.
[5] W. Wiese, B. Emonts, R. Peters, J. Power Sources 84 (1999) 187.
[6] P. Kumar, Fuel Cell Handbook, 5th ed., US Department of Energy, 2000.
[7] S. Gottesfeld, J. Pafford, J. Electrochem. Soc. 135 (10) (1998) 2651–2652.
[8] D.P. Wilkinson, H.H. Voss, J. Dudley, G.J. Lamont, V. Basura, Patent No. WO95/08850 (1995).
[9] F.A. de Bruijn, D.C. Papageorgopoulos, E.F. Sitters, G.J.M. Janssen, J. Power Sources 110 (2002) 117–213.
[10] J.J. Baschuk, X. Li, Int. J. Energy Res. 27 (2003) 1095–1116.
[11] G. Karimi, J.J. Baschuk, X. Li, J. Power Sources 147 (2005) 162–177.
[12] J. Newman, Electrochemical Systems, 2nd ed., Prentice-Hall, New Jersey, 1991.
[13] G.C. Chinchen, P.J. Denny, J.R. Jennings, M.S. Spencer, K.C. Waugh, Appl. Catal. 36 (1988) 1–65.
[14] J.J. Baschuk, X. Li, Int. J. Global Energy Issues 20–23 (2003) 245–276.
[15] T. Zawodzinski, C. Karuppaiah, F. Uribe, S. Gottesfeld, Electrochem. Soc.: Pennington (1997) 139–146.
[16] J.J. Baschuk, X. Li, Int. J. Energy Res. 28 (2004) 697–724.